Received: 21 September 2020 | Revised: 25 February 2021 | Accepted: 2 March 2021

DOI: 10.1002/rcm.9078

RESEARCH ARTICLE

Rapid Communications in Mass Spectrometry WILEY

Continuous and simultaneous measurement of triple-oxygen and hydrogen isotopes of liquid and vapor during evaporation experiments

Matthew P. Brady | David A. Hodell

Godwin Laboratory for Paleoclimate Research, Department of Earth Sciences, University of Cambridge, Downing Street, Cambridge, CB2 3EQ, UK

Correspondence
M. P. Brady, Godwin Laboratory for Paleoclimate Research, Department of Earth Sciences, Downing Street, University of Cambridge, Cambridge CB2 3EQ, UK.
Email: mpb68@cam.ac.uk

Funding information
Natural Environment Research Council, Grant/Award Number: NE/L002507/1; ERC WHIM, Grant/Award Number: 339694

Rationale: Oxygen and hydrogen isotopes are important tools for studying the modern and past hydrological cycle. Previous evaporation experiments used episodic measurement of liquid and/or vapor or did not measure all isotopologues of water. Here, we describe an evaporation experimental system that allows all isotopologues of liquid and water vapor to be measured simultaneously and near-continuously at high precision using cavity ring-down laser spectroscopy (CRDS).

Methods: Evaporating liquid is periodically sampled from a closed recirculating loop by a syringe pump that delivers a constant supply of water to the vaporizer, achieving a water vapor concentration of 20,000 ppmV H_2O (±132, 1σ). Vapor is sampled directly from the evaporation chamber. Isotope ratios are measured simultaneously with a Picarro L2140-*i* CRDS instrument.

Results: For liquid measurements, Allan variance analysis indicates an optimum data collection window of 34 min for oxygen isotopes and 27 min for hydrogen isotopes. During these periods, the mean standard error is ±0.0081‰ for $\delta^{17}O$ values, ±0.0081‰ for $\delta^{18}O$ values, and ±0.019‰ for $\delta^{2}H$ values. For the derived parameters ^{17}O-excess and d-excess, the standard error of the mean is 5.8 per meg and 0.07‰, respectively. For the vapor phase a 12.5 min data window for all isotopologues results in a mean standard error of ±0.012‰ for $\delta^{17}O$ values, ±0.011‰ for $\delta^{18}O$ values, and ±0.023‰ for $\delta^{2}H$ values. For the derived parameters, the standard error of the mean is 9.2 per meg for ^{17}O-excess and 0.099‰ for d-excess. These measurements result in consistently narrow 95% confidence limits for the slopes of $\ln(\delta^{17}O + 1)$ vs $\ln(\delta^{18}O + 1)$ and $\ln(\delta^{2}H + 1)$ vs $\ln(\delta^{18}O + 1)$.

Conclusions: The experimental method permits measurement of fractionation of triple-oxygen and hydrogen isotopes of evaporating water under varying controlled conditions at high precision. Application of this method will be useful for testing theoretical models of evaporation and conducting experiments to simulate evaporation and isotopic equilibration in natural systems.

1 | INTRODUCTION

The movement of water in the hydrological cycle is largely dominated by evaporation and condensation processes. Oxygen and hydrogen stable isotopes (^{1}H, ^{2}H, ^{16}O, ^{17}O, and ^{18}O) of water undergo fractionation during evaporation and precipitation as a consequence of both kinetic and equilibrium effects.[1] A variety of evaporation experiments have been conducted in an attempt to understand and quantify these effects.[2–9] In all previous experimental designs, sampling of the liquid undergoing evaporation and its resulting vapor has been episodic and relatively infrequent. The liquid and the vapor have been sampled at discrete times during the course of the experiment, resulting in a relatively small number of measurements. Incident vapor has been collected for measurement by freezing or trapping,[10] thereby increasing procedural complexity and the opportunity for error.

Most experiments included measurements of $\delta^{18}O$ and $\delta^{2}H$ values by dual-inlet isotope ratio mass spectrometry (DI-IRMS). Oxygen isotopes are typically measured by isotope exchange with CO_2 and hydrogen isotopes by reduction with a metal (Ni, Cr, or U).[11–13] However, $\delta^{17}O$ values have rarely been measured and traditionally involve fluorination of H_2O to produce O_2.[14] Recent developments in laser absorption technology now permits continuous measurements of all stable isotopes of oxygen and hydrogen in liquid water and vapor with precisions comparable with, or exceeding, conventional IRMS methods.[15] This technological advance opens up new opportunities for studying isotope fractionation during evaporation, which hitherto has been extremely laborious.

Measurement of singly substituted isotopologues of water (i.e. $^{1}H^{2}H^{16}O$, $^{2}H_2{}^{16}O^{18}O$, and $^{2}H^{16}O^{17}O$) relative to the abundant (i.e. $^{1}H_2{}^{16}O$) permits calculation of the derived parameters d-excess and ^{17}O-excess, which are defined as:

$$\mathrm{d-excess} = \delta^{2}\mathrm{H} - 8 \times \delta^{18}\mathrm{O} \quad (1)$$

and

$$^{17}\mathrm{O-excess} = \ln\left(\delta^{17}\mathrm{O} + 1\right) - \lambda \times \ln\left(\delta^{18}\mathrm{O} + 1\right) \quad (2)$$

where λ is estimated to be 0.528 for unevaporated natural waters.[16] Using multiple isotopes to trace fractionation processes provides distinct advantages for both testing theoretical models and their application to hydrologic problems.

Here, we report an experimental design that permits the measurement of all stable isotopes of liquid water and resulting vapor upon evaporation at a sampling frequency that is more than an order of magnitude greater than most previous experiments. This is achieved by coupling an evaporation chamber directly to a L2140-*i* cavity ring-down spectroscopy (CRDS) instrument (Picarro, Santa Clara, CA, USA). The main advantage is the large number of measurements made over the course of an evaporation experiment, exceeding 100,000 for each isotope. Such large datasets result in very low standard errors of the mean for single isotope ratios and small errors on regression equations when comparing multiple isotope ratios. The method provides a detailed description of the fractionation curves for both the liquid and vapor as a fraction of the water remaining for all stable isotopes, thereby permitting fraction factors to be estimated throughout the course of the experiment.

2 | EXPERIMENTAL

2.1 | System hardware

The proposed experimental system is divided into two parts: the first is the chamber where evaporation takes place and the second is the sampling and isotopic measurement of liquid and vapor phases by CRDS. The evaporation chamber consists of a sealed glove box (approximately 0.23 m^3) containing a pan of water resting on a balance, which monitors weight loss over the course of an experiment (see sections SI1 and SI5, supporting information). Relative humidity (RH) and temperature are measured continuously using a single temperature/RH probe (4185CC; Traceable Products, Webster, TX, USA) that is positioned 10 cm above the evaporating fluid. All electrical cables and tubing are passed into the glovebox through a sealed silicone plug. Dry air is supplied from a compressed gas cylinder with a two-stage regulator set at 1.5 bar pressure. The flow rate of gas to the chamber is controlled using a 12-turn metering valve (Swagelok, Solon, OH, USA).

The interface to the Picarro L2140-*i* consists of heated 1/4″ diameter stainless steel tubing that exits the chamber through the silicone plug. It is configured with a T-connector in line that serves as an open split with one end open to atmosphere and the other connected to the inlet of an A0211 vaporizer (Picarro) via heated 1/8″ steel tubing. This configuration permits the Picarro analyzer to draw the flow it requires (~35 mL min^{-1}) and prevents the over-pressurization of the glove box. Flow rate from the open split is monitored at the beginning of each experiment to ensure that there is no backflow into the glove box or analyzer.

Downstream of the glovebox, the system is dedicated to the sampling and measuring the experimental liquid and vapor. Water from the evaporation pan is continually recirculated through a loop consisting of PFA tubing (G180-65105, Agilent Technologies, Santa Clara, CA, USA), with flow driven by a peristaltic pump (IPC, Ismatec, Wertheim, Germany) fitted with Tygon Standard R-3607 (orange-orange SC0009) tubing. The pump circulates water at a rate of 1.25 mL min^{-1} over a total tube length of ~2.5 m. The total volume of the loop is ~0.5 mL. The ends of the recirculation loop are submerged and almost flush with the base of the evaporation pan; the maximum replacement time for this water is 64 min. Water is sampled from the loop for measurement through a T-junction that is connected to one of the syringe pumps of the standards delivery module (SDM; A0101, Picarro). The syringe pump delivers liquid water to the vaporizer at a low flow rate to

achieve constant water vapor concentration in the analyzer cavity. For a single injection during an experiment, the syringe pump draws 140 μL of water into the syringe from the recirculating loop and injects this water to the vaporizer, set at 140°C, as is standard for SDM operation.

The method alternates between analysis of the liquid (from the syringe pumps) and vapor sampled from the evaporation chamber. The vapor from the evaporation chamber enters the L2140-*i*, bypasses the vaporizer and flows directly to the analyzer cavity, thereby minimizing memory effects between the liquid and vapor phases – which have significantly different isotopic ratios. In the SDM, one syringe pump is utilized to monitor the evaporated water, and the other is connected to a standards delivery bag to monitor instrument drift over the course of an experiment. For correct $\delta^{17}O$ measurement of the vapor from the evaporation chamber, it is essential that the water-free air used as the carrier gas should be the same for the glove box and the SDM for proper background correction. The SDM air is supplied from a glove bag that is filled by the same dry gas type that is supplied to the evaporation chamber. A schematic of the system is given in Figure 1 and photographs of the system in a lab context are provided in section SI1 (supporting information).

2.2 | Instrumental drift

To monitor and correct for instrument drift over the course of an experiment, we introduce a water standard with known isotopic ratios at regular intervals (~15 h), including at the start and end of the experiment. The injections of the drift standard follow the same structure as the standard injections (see section 2.3). For a drift correction to be applied, one of the following criteria must be met: a clear trend in the drift standard isotope ratios is observed; i.e., total change in the measurements is greater than the threshold values (<0.2‰ $\delta^{17}O$, <0.3‰ $\delta^{18}O$, and <1.5‰ $\delta^{2}H$) over the course of an experiment.

If these criteria are met, linear regressions are applied to each isotope ratio, and the gradient, γ, is recorded throughout the length of the experiment. To correct the experimental data and initial and final standards the following calculation is applied:

$$\delta^{*}_{dc} = \delta^{*}_{m} - \text{time} \cdot \gamma \quad (3)$$

where δ^{*}_{dc} is the drift-corrected value, δ^{*}_{m} is the measured value, and the time is in minutes (min). It is only after the drift corrections have been made that the data are calibrated to the VSMOW-SLAP scale.

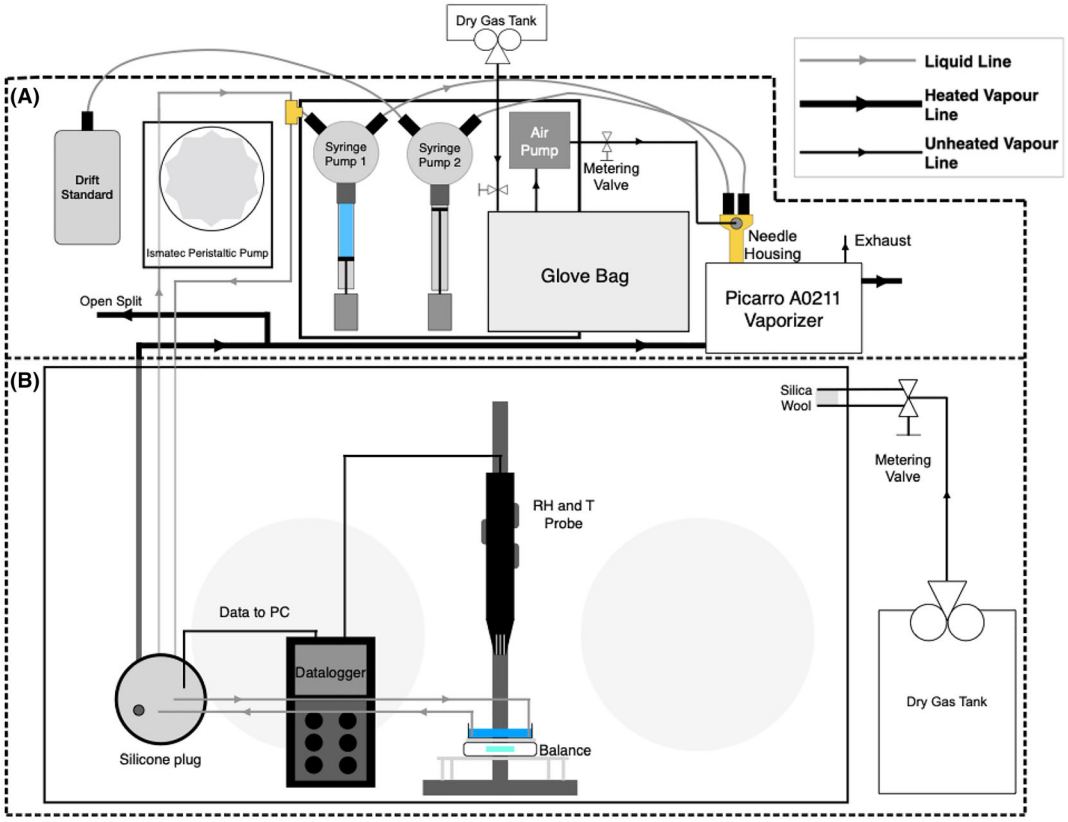

FIGURE 1 Experimental schematic. Dashed box **A** show the sampling and measurement part of the system, with water recirculation driven by the peristaltic pump, and sampling and injection to the vaporizer carried out by the SDM. The true layout minimizes the distances between syringe pump 1 and the needle housing and the heated vapor line to the vaporizer. Dashed box **B** shows the experimental part of the system with water evaporating from a dish set on a balance. Relative humidity is recorded by the probe mounted on a ring stand, which is set 10 cm above the surface of the water, and controlled by adjusting the metering valve. The box is sealed and liquid, vapor, and data cables exit the box through a silicone plug. The design of dashed box **B** can be adapted as required

2.3 | Calibration procedure

The Picarro water isotope analyzer is calibrated using two in-house standards (MPB Enr and JRW; values in Table 1) that are, in turn, calibrated to the VSMOW-SLAP scale. The standards bracket the range of liquid and vapor delta values encountered during the course of an evaporation experiment and are run at the beginning and end of an experiment.

We used a measurement sequence that included injection rates from the syringe pumps of 0.05 μL s^{-1} and 0.03 μL s^{-1} (targeting 20,000 ppm and 12,500 ppm H_2O, respectively) for 40 min for each standard. These different concentrations are used to define the concentration dependence of the delta values. This concentration-corrected calibration is applied to the vapor data, whose concentration in the cavity is dependent on the target RH in the evaporation chamber.

A drift standard is analyzed every 15 h throughout the course of the experiment. After applying the drift correction (see section 2.2) to the measured delta values of both the calibration and the experiment data, we apply a linear correction of the form:

$$\delta^*_{cal} = \frac{\delta^*_{meas\ dc} - c^*_{corr}}{m^*_{corr}} \quad (4)$$

where δ^*_{cal} is the calibrated isotope ratio of interest, and $\delta^*_{meas\ dc}$ is the (drift-corrected) measured isotope value of interest. We plot the VSMOW-SLAP calibrated isotope ratio of the two standards (x-axis) on the SLAP-VSMOW scale versus the measured and drift-corrected isotope ratios (y-axis) and calculate a slope (m^*_{corr}) and intercept (c^*_{corr}).

2.4 | Experimental sequence

Prior to the start of an experiment, the evaporation chamber is purged and dried overnight to <5% RH (which corresponds to <2500 ppmV H_2O recorded in the CRDS analyzer) using a flow of dry air. Initially, 80 g of water is placed in the evaporation pan and the peristaltic pump is turned on to circulate water through the sampling loop. The gas flow is continuously adjusted to obtain the desired RH, which is achieved after an equilibration period of up to 2000 min (~33 h) for high RH experiments. The starting point of an experiment is defined when the 5 min averaged RH gradient falls below 0.1% s^{-1}.

We target 20,000 ppmV H_2O for the liquid injections with a flow rate of 0.05 μL s^{-1} from syringe pump 1 for 40 min. The syringe pump utilizes ~140 μL of water from the evaporation pan every 88 min. At the end of each injection, dry gas continues to flow through the vaporizer, lowering the measured H_2O concentration in the cell to ~1700 ppmV. Measurement of the liquid alternates with the ambient vapor from the evaporation chamber, also for 40 min. The high stability of the CRDS systems means that a drift standard has to be introduced infrequently.[17] Here, syringe pump 2 injects a drift standard every ~15 h. The start of a typical experimental sequence is highlighted in Figure 2.

The experiment continues until the surface area of the evaporating water no longer covers the entire area of the evaporating pan at which time the RH declines because the water vapor in the chamber is entirely provided by evaporation of the liquid. The total time for an experiment depends on the target RH and can vary from 5 to 15 days.

3 | RESULTS AND DISCUSSION

3.1 | Stability and Allan variance

To determine long-term system stability and select the ideal length of time for injection, Allan variance was calculated by repeatedly measuring isotope ratios of a large, sealed volume of isotopically homogeneous water for 42 h.[18] Deionized water was sampled using the syringe pump from a recirculating loop, with injections lasting 30 min each and repeated over 2500 min. Triple-oxygen and hydrogen isotope data were recorded every ~1.5 s, corresponding to a frequency of ~0.67 Hz. A small amount of data was ignored each time that the syringe pump was refilled in order for equilibration to be obtained in the vaporizer and cavity. After the removal of these data, 87,625 data points remained from a total of 101,158 measurements (Figure 3). The long-term stability of each parameter is estimated by the total standard deviations (1σ): ±132 ppmV for H_2O concentration, ±0.29‰ for $\delta^{17}O$ values, 0.26‰ for $\delta^{18}O$ values, and 0.57‰ for δ^2H values over the 2500 min period. No drift correction was applied. These results agree with the stability reported by Gkinis et al who conducted a similar experiment for $\delta^{18}O$ and δ^2H using a Picarro L2130-*i* over a 17-h period.[19]

Allan variance was calculated using the allanvar function in MATLAB (mathworks.com/help/nav/ref/allanvar.html). The Allan variance decreases for all isotopes reaching a minimum plateau (the noise floor) and then increases again with time (Figure 4) owing to longer-term drift of the instrument. For $\delta^{17}O$ and $\delta^{18}O$ values, the noise floor occurs between integration times of 2000 s (33.3 min) and 6800 s (113 min), broadly consistent with previous estimates of optimal time (τ_{opt}) using the L2140-*i* CRDS instrument.[15,20,21] The minimum σ_{Allan} values calculated for $\delta^{17}O$ and $\delta^{18}O$ across this

Standard	$\delta^{17}O$ (1σ)	$\delta^{18}O$ (1σ)	δ^2H (1σ)	^{17}O-excess (1SEM)
JRW	−9.99 (0.04)	−18.90 (0.04)	−146.51 (0.19)	32 (12)
MPB Enr	15.58 (0.03)	29.97 (0.04)	89.25 (0.19)	−136 (6)

TABLE 1 Calibration standard values. These values were determined using the method outlined in Schoenemann et al[17] σ is the standard deviation and SEM = $\sigma/\sqrt{n}$

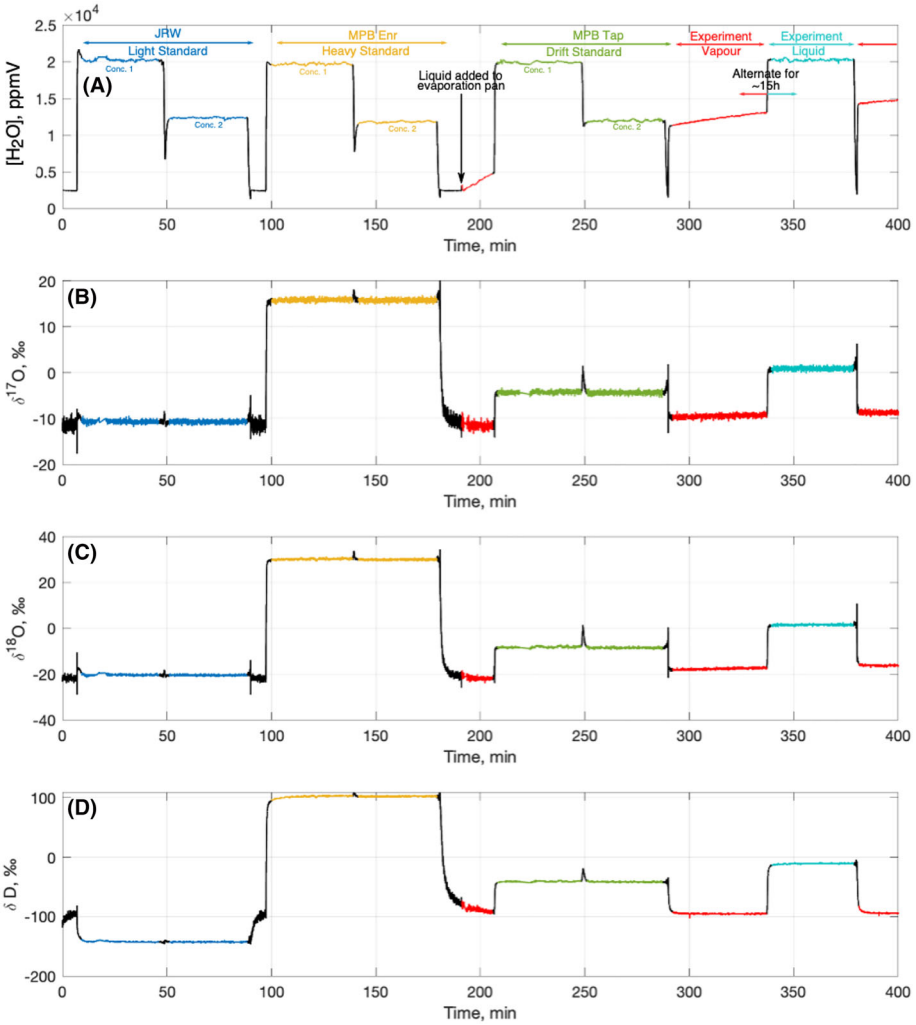

FIGURE 2 Output from the L2140-*i* analyzer at the start of an evaporation experiment. Colored windows represent a source of different liquid or vapor being introduced into the analyzer. First, the isotopically light (blue) and isotopically heavy (yellow) in-house standards are measured followed by the drift standard. Henceforth, the analysis switches Experimental Vapor (red) and Experimental Liquid (light blue) with the occasional introduction of the drift standard (not shown). At the end of the experiment, the calibration is repeated as per the beginning of the analysis

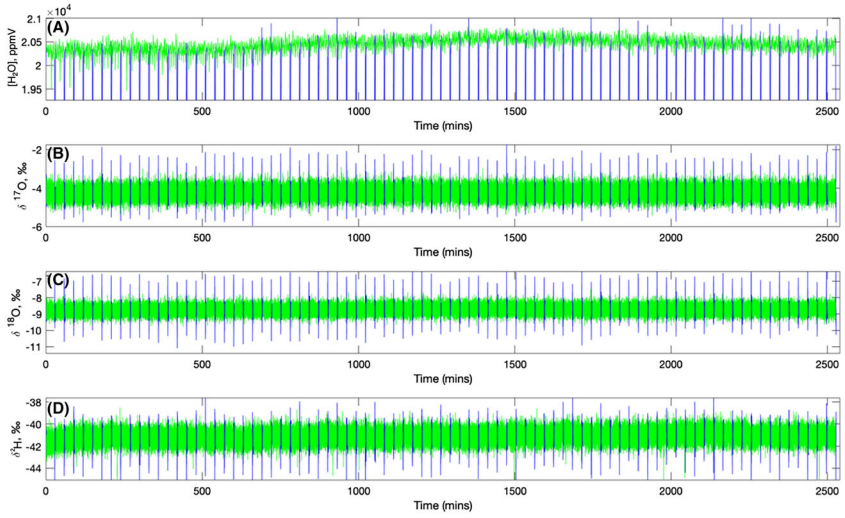

FIGURE 3 Continuous injection data for Allan variance analysis. The whole dataset (blue) has been cropped to remove the equilibration time required between each injection, leaving only the data used to calculate the Allan variance (green). The standard deviations shown are calculated from the processed (green) data. Note, this is not an evaporation experiment

interval are 0.008‰ and 0.009‰, respectively. When the $\delta^{17}O$ and $\delta^{18}O$ values are combined to give the ^{17}O-excess, the Allan variance across the noise floor is 5.5 to 6.0 per meg. Achieving the noise floor for $\delta^{2}H$ values requires shorter integration times than for $\delta^{18}O$ and $\delta^{17}O$ values, with τ_{opt} spanning the intervals of 570 s (9.5 min) to 1800 s (30 min), with a minimum σ_{Allan} = 0.051‰. To maximize precision in $\delta^{2}H$ measurements we use a shorter integration window than that used for the oxygen isotopes.

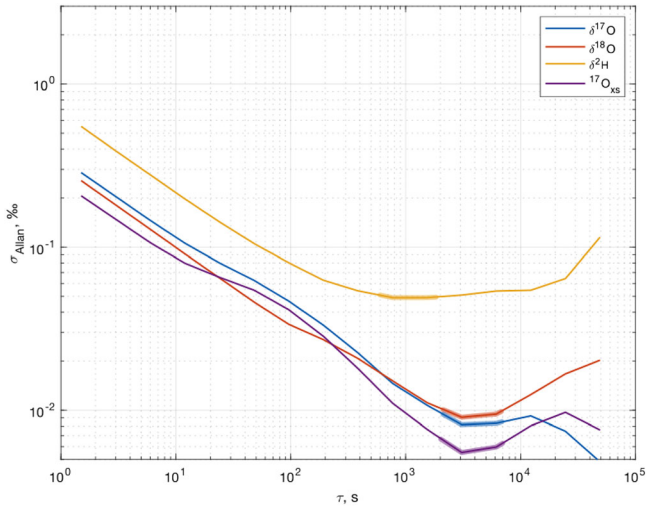

FIGURE 4 The Allan deviation, σ_{Allan}, calculated for continuous injection to the vaporizer over a 42-h period. The shaded areas define the optimum integration windows

The minimum of the Allan variance plateau is the best precision obtainable on a liquid water sample if sufficient quantities (<10 mL) are available for measurement. There are cases when such ultra-precise measurements may be desirable; for example, when the amount of water is unlimited and variations in the samples being studied are very small.

3.2 | Liquid measurements

Measurements of the evaporating water are made by sampling a loop containing recirculating liquid from the evaporation pan. Memory from the previous sample (which can be a liquid or vapor) is a potential problem that can significantly affect the precision of isotopic measurements in CRDS systems.[17] Memory effects are greatest at the beginning of each liquid injection where a small amount of water remains in the system from the previous sample. At the target pump rate of 0.05 μL s^{-1}, data for the initial 4 min of each liquid injection are discarded. To ensure that memory effects have been overcome, we then disregard the next 2 min of injection data for the oxygen isotopologues (34 min of usable data). Since memory effects are more severe for hydrogen isotopes, we ignore the next 13 min of data (27 min of usable data) in order to take advantage of the shorter integration period required to achieve the Allan variance minimum for δ^2H values. More detail about the length of these windows is given in section SI3 (supporting information).

The precision of isotope measurements on the liquid water undergoing evaporation is estimated in Table 2 using both the standard deviation and the standard error of the mean (SEM). The SEM is very low because of the large values of n and is the more appropriate estimate of uncertainty about the mean value.

TABLE 2 The average standard deviation, σ, and standard error of the mean, SEM = $\sigma/\sqrt{n}$, of liquid measurement periods during a typical experiment after memory windows have been removed. n = ∼1370 for oxygen isotopologues and n = ∼1100 for deuterium. Number of injections = 72

Measurement	Av. measurement σ	Av. measurement SEM
$\delta^{17}O$	0.28‰	0.0081‰
$\delta^{18}O$	0.25‰	0.0076‰
$\delta^{2}H$	0.61‰	0.019‰
^{17}O-excess	210 per meg	5.8 per meg
d-excess	2.4‰	0.07‰

3.3 | Vapor measurements

During the course of an experiment, the analysis continually switches between measurement of the liquid and vapor. Unlike the liquid measurements which require a previous sample to pass through the analyzer before the removed sample is measured, vapor measurements are made into a dry cavity with almost no sample overlap. It is common to characterize the response of the CRDS analyzer cavity to a change in concentration and isotopic ratios as a transfer function and impulse response. For the transition between liquid and vapor, we calculate an impulse response of the instrument (σ_{IR}) of ∼35 s for all three isotopes, leading to data removal for the initial 105 s (see section SI3, supporting information), resulting in an ∼38.5 min data collection window for vapor-phase measurements.

Whilst this data removal appropriately deals with the transition period at the beginning of the vapor measurement, there was an observed increase in the isotopic ratio within the 38.5 min collection window, especially as evaporation progressed. This suggests that the rate of change in isotopic composition was faster than the length of the measurement window towards the end of the experiment, occurring because of the greater isotopic difference between the liquid and vapor with increased evaporation. To account for this, the data collection period was optimized such that its length minimizes slope increases and is sufficiently long to allow for the ^{17}O-excess SEM to be ≤10 per meg. A 750-s window (12.5 min, ∼500 measurements) is optimal. This results in approximately three measurements of the vapor for every liquid-phase measurement (Figure 6).

The precision of vapor measurements achieved in a typical experiment is shown in Table 3. The average isotopic gradients over a 12.5 min period result in negligible increases in the oxygen isotopes and an average increase of 0.18‰ in the δ^2H value. The standard deviation precision achieved for all isotope systems is comparable with that achieved on liquid-phase measurements. However, due to the shorter measurement window, the SEM precisions for vapor-phase measurements are not as good as for liquid-phase measurements, despite being able to achieve <10 per meg in ^{17}O-excess.

TABLE 3 The average gradient and standard deviations, σ, and standard error of the mean, SEM = $\sigma/\sqrt{n}$, of vapor measurement periods during a typical experiment with ~20,000 ppmV H_2O. $3\sigma_{IR}$ data removal and window length optimization have been applied. n = ~500 data points for each measurement window. Number of measurements = 216. *per meg min^{-1}

Measurement	Av. measurement gradient, ‰ min^{-1} (1σ)	Av. measurement σ	Av. measurement SEM
$\delta^{17}O$	$1.9x10^{-4}$ (0.0046)	0.28‰	0.012‰
$\delta^{18}O$	$2.3x10^{-5}$ (0.0053)	0.25‰	0.011‰
$\delta^{2}H$	−0.014 (0.024)	0.52‰	0.023‰
^{17}O-excess	0.0017 (3.5)*	206 per meg	9.2 per meg
d-excess	−0.014 (0.044)	2.2‰	0.099‰

3.4 | Evaporation experiments

The evolution of the isotopic composition of water was studied as it evaporated under three relative humidity settings: 26.8 (0.9)%, 34.2 (1.9)%, and 55.5 (1.0)% RH (±1σ), and constant temperature 19.1 (±0.26)°C, 19.6(±0.26)°C, and 21.2(±0.16)°C, respectively. Figure 5 shows how δ-values changed as evaporation progressed, and the fraction of water remaining, *f*, decreases at RH = 34.2%. The data are fitted with an equation of the form:

$$\delta^{*} = A \cdot \ln(f) + B \tag{5}$$

where A and B are constants derived using least-squares regression. Constants for all three experiments are given in section SI4 (supporting information). For any value of *f* during an evaporation experiment, the fractionation factor, $^{*}\alpha_{evap}$, is given by:

$$^{*}\alpha_{evap} = \frac{^{*}R_w}{^{*}R_V} = \frac{^{*}\delta_w + 1000}{^{*}\delta_v + 1000} \tag{6}$$

where $^{*}\alpha_{evap}$ is the fractionation factor for the isotope of interest, *, and $^{*}R_w$ and $^{*}R_v$ are the isotopic ratios of the evaporating liquid and measured vapor, respectively.[22] With both the liquid and the vapor measured, the fractionation factor can be calculated continuously over the course of an experiment. For the experiment shown, the fractionation factor decreases throughout the course of the experiment by ~5% for both oxygen isotopes and increases by ~3% for ^{2}H, when converted to their 1000Ln($^{*}\alpha_{evap}$) approximations (Figure 5). In fact, the observed change in the fractionation factor during our experiments was insignificant at the 2σ confidence level, when errors are propagated from the isotopic ratio measurements (Tables 2 and 3; Figure 5).

In addition to evaporative trends as a function of the remaining liquid fraction for individual isotope ratios, it is useful to examine the gradients of different isotope systems, e.g. $\delta^{17}O$ vs $\delta^{18}O$ and $\delta^{2}H$ vs $\delta^{18}O$.[7,23,24] For all experiments, the 95% confidence interval (CI) on the slopes of ln($\delta^{17}O$ + 1) vs ln($\delta^{18}O$ + 1) is better than 0.0004 for liquid-phase measurements and 0.0006 for vapor-phase measurements. For $\delta^{2}H$ vs $\delta^{18}O$, the 95% CI on the slope is better than 0.047 and 0.029 for the liquid and vapor phases, respectively.

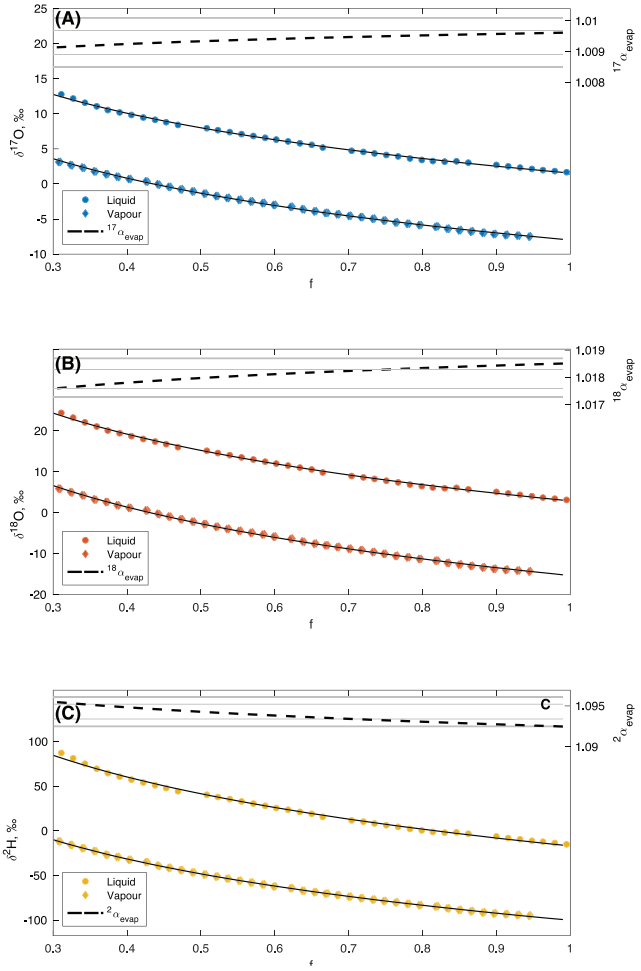

FIGURE 5 Isotopic evolution for A, $\delta^{17}O$ values; B, $\delta^{18}O$ values; and C, $\delta^{2}H$ values for an evaporation experiment conducted at 34.2% RH. The solid lines are curve fits of the form of Equation 5 and are used to calculate the isotopic ratio and fractionation factor at each injection time. The dashed line is the $^{*}\alpha_{evap}$ value (Equation 6) of the experiment as evaporation proceeds. The horizontal lines are the errors calculated for $^{*}\alpha_{evap}$ at 1σ (thin grey) and 2σ (thick grey) significance. These errors are calculated by propagating the error for the measurements of isotope ratios in the liquid and vapor (Tables 2 and 3). Periodic gaps in data are when the drift standard is introduced into the system. Each point in the liquid evolution is the average of continuous data over 34 min (see section 3.2) and each vapor data point represents a 12 min integration window (see section 3.3)

The slopes and confidence limits produced using the new method are shown in Table 4, alongside data from previously published evaporation experiments.

The slope of δ^2H-δ^{18}O is dependent on the conditions under which the evaporation occurs (e.g. temperature, humidity, wind speed, etc.). The slopes of the evaporation experiments increased from 4.472 to 5.282 for the liquid and from 3.830 to 4.471 for the vapor, as the RH increased (Table 4, Figure 6). These relationships are consistent with predictions of increasing slope of the evaporation line as RH increases.

The slope of $\ln(\delta^{17}O + 1)$ vs $\ln(\delta^{18}O + 1)$ is primarily a function of the RH as the temperature was near constant during each of the experiments.[26] The 95% CI of the calculated slope is often better than 0.0005 because of the large value of n. Knowing the value of this slope at high precision is important as the maximum possible variability in this slope at 21°C is 0.0055 (increasing to 0.006 at

TABLE 4 Precision of slopes produced for evaporation experiments conducted in this study under a range of conditions. The slopes and precisions quoted are calculated using published data and the MATLAB Curve Fitting application (mathworks.com/help/curvefit/curvefitting-app.html)

	RH, %	T, °C	No. of samples	$\ln(\delta^{17}O + 1)$ vs $\ln(\delta^{18}O + 1)$ slope	95% CI	δ^2H vs δ^{18}O slope	95% CI
This study	26.6	19.1	39 (liq.)	0.5266	0.0003	4.472	0.029
			122 (vap.)	0.5250	0.0005	3.830	0.024
	34.2	19.6	40 (liq.)	0.5256	0.0003	4.735	0.037
			129 (vap.)	0.5246	0.0005	4.103	0.021
	55.5	21.3	36 (liq.)	0.5249	0.0005	5.282	0.041
			128 (vap.)	0.5231	0.0005	4.471	0.021
Cappa et al[10]	51.2	19.4	6 (liq.)	-	-	4.769	0.289
			6 (vap.)	-	-	4.207	0.655
	51.4	20.0	7 (liq.)	-	-	4.717	0.219
			7 (vap.)	-	-	4.018	0.451
	20.4	20.1	6 (liq.)	-	-	4.742	0.081
			6 (vap.)	-	-	4.079	0.292
	0	20.4	5 (liq.)	-	-	4.166	0.146
			4 (vap.)[a]	-	-	3.977	0.329
	0	19.3	4 (liq.)	-	-	4.586	0.415
			3 (vap)[a]	-	-	4.158	0.658
Barkan and Luz[3]	0.0067[e]	25	3	0.5254	0.0041	-	-
	0.0135	40	5	0.5253	0.0003	-	-
Luz et al[5]	0.0419	69.5	4	-	-	1.943	0.697
	0.0274	39.8	4	-	-	2.362	0.023
	0.0241	20.1	4	-	-	2.862	0.112
	0.0195	10.0	5	-	-	3.213	0.157
Steig et al[15]	low	N/A	42	0.5232	0.0004	-	-
Skrzypek et al[8]	29.2	24.8	14	-	-	4.673	0.098
	22.2	32.6	12	-	-	4.055	0.113
	22.2	32.6	12	-	-	4.028	0.143
	22.2	32.6	12		-	4.147	0.087
Surma et al[7]	20	25	5	0.5253	0.0005	-	-
	50	25	5	0.5251	0.0005	-	-
	80	25	5	0.5264	0.0019	-	-
Gonfiantini et al[9f]	25.5	22.0	9	0.5287	0.0028	2.699	0.033
Gonfiantini et al[25]	26.2[g]	24.5	6	-	-	3.410	0.148
	27.3	24.1	15	-	-	3.757	0.099

[a]To calculate comparable slopes and precision, one data point has been removed.
[e]The average of the three replicates was used for each measurement.
[f]Their experiment 1.
[g]Their experiments 2 and 8.

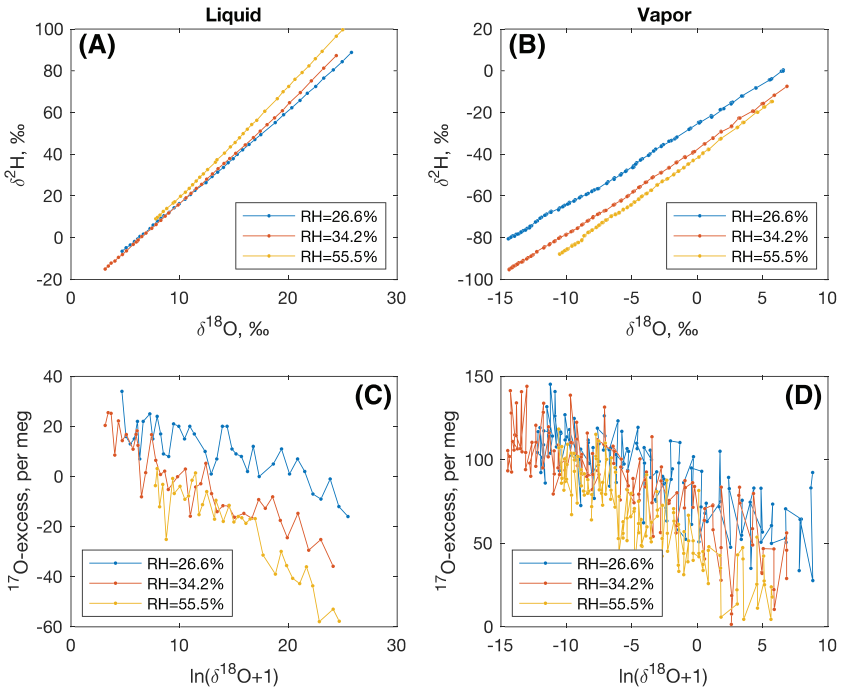

FIGURE 6 The systematics of δ^2H-δ^{18}O of A, liquid and B, incident vapor undergoing evaporation, alongside the ^{17}O-excess-ln (δ^{18}O + 1) in C, the liquid and D, the vapor. The offset between initial vapor values observed in B is the result of the different fractionation factors under varying RH conditions, despite using the same starting liquid

TABLE 5 The mol fractions of water between the liquid and vapor phase of each experiment at initiation and termination, assuming that conditions are homogeneous within the box. Also shown is the percentage change $^*\alpha_{evap}$ of each experiment (in the form 1000Ln($^*\alpha_{evap}$))

RH, %	Initial $H_2O_{l/v}$ mol fraction	End $H_2O_{l/v}$ mol fraction	%Δ $^2\alpha_{evap}$	%Δ $^{17}\alpha_{evap}$	%Δ $^{18}\alpha_{evap}$
26.6	74.4	22.3	7.6	−2.1	−2.5
34.2	58.0	17.4	3.1	−5.1	−5.4
55.5	35.9	10.8	4.5	2.5	2.1

40°C).[7] Therefore, to consistently achieve a 95% CI precision that is appropriate for investigating evaporation under a range of conditions, it is desirable to perform a large number of measurements.

The derived parameter ^{17}O-excess is a relatively new tool for examining the hydrological history of terrestrial waters and precipitated minerals.[6,23,27] As evaporation increases, the value of ^{17}O-excess decreases. Figures 6C and 6D show a decrease of the ~50 per meg in the ^{17}O-excess as a function of ln(δ^{18}O + 1). The 95% CI for the slopes of these curves in the liquid and vapor phase is better than 0.49 and 0.55, respectively. Although there is considerable variability from one measurement to the next, the slopes are fairly well constrained, suggesting the method will be useful for conducting experiments into the use of ^{17}O-excess as a hydrologic tracer.

3.5 | Design of the evaporation chamber and experiments

Controlled experiments are important for understanding isotope fractionation including both kinetic and equilibrium effects that can occur during evaporation. In this study, we focused mainly on the isotopic measurements of the liquid and vapor (e.g. the precision of isotopic measurement and slope confidence intervals), rather than the specific results of the experiments that are dependent upon the design and purpose of the evaporation chamber.

In our experiment, the replacement time of gas in the box is dependent on the gas flow rate that is used to set the RH. This results in a different residence time in the box for each experiment. Based on the gas flow for the 26.6%, 34.2%, and 55.5% RH experiments, the residence times are ~170 min, ~200 min, and ~390 min, respectively. This results in a system that is not completely open, where the instantaneous isotopic composition of the liquid is out of equilibrium with the vapor. The offset between the liquid and the vapor could result in small changes being observed in the $^*\alpha_{evap}$ values as an experiment progresses. The oxygen isotope fractionation factors for the 26.6% and 34.2% RH experiments decreased by ~2% and ~5% in the 100Ln($^*\alpha_{evap}$) form, respectively (Table 5). These small decreases in the fractionation factor are probably the result of back equilibration between the vapor in the chamber and the evaporating pan, permitted by the long residence times in the box. As such, it is expected that the largest negative offset would be for the experiment in which the residence time in the box is the longest and the RH is highest. However, the fractionation factors for the oxygen isotopes for the 55.5% RH experiment increase by 2.5% and 2.1% as evaporation progresses (Table 5). The increase in oxygen isotope

fractionation factors is ascribed to the considerably lower $mol(H_2O)_{liq}/mol(H_2O)_{vapor}$ of this experiment (Table 5), which permits the instantaneous isotopic ratio of the liquid water to change more quickly than that of the measured vapor as evaporation proceeds, tempering and reversing the decrease in fractionation factor driven by back-equilibration. Other processes that become more significant at higher RH (e.g. water adsorbing to evaporation chamber surfaces) may also have a role and may explain the positive offsets observed for the hydrogen isotope fractionation factors observed in each experiment (Table 5). Another possibility is that the small changes in the fractionation factor are related to instrument drift that is not fully corrected for by our drift correction procedure, which could explain why the direction of change differs for oxygen and hydrogen isotopes in some experiments. Despite these caveats, we emphasize that the change in the calculated fractionation factors during our experiments is insignificant at the 2σ confidence level when errors are propagated from the isotope ratio measurements. Better constraints on chamber conditions could be provided by a network of hygrometers, and future work would benefit from monitoring the temperature of the evaporating fluid. Ideally, temperature should be measured at the air–water interface as this can be critical for precise examination of evaporation trends.[3,28]

The sampling and measuring routine described above is adaptable to almost any two-phase liquid and vapor system. There may also be cases where the user might want to continuously monitor the liquid only, and not the vapor. For example, using a different carrier gas (other than N_2 or dry air) that is incompatible with the Picarro CRDS instrument.[5] It may also be desirable to add water vapor with a known isotopic composition to the chamber so that the vapor is not simply produced by the evaporating water, while still controlling other variables.

3.6 | Modelling evaporative trends

Critical to the experimental setup is its ability to recreate evaporative trends that can be used to model real-world systems or interpret paleohydrologic data, particularly the derived hydrological tracers ^{17}O-excess and deuterium excess.

The model trajectory for each of the isotope species is described by a simple Rayleigh fractionation[22]:

$$ {}^{*}R = {}^{*}R_o f^{\left(1/{}^{*}\alpha_{evap}-1\right)} \quad (7) $$

where $^{*}R$ is the instantaneous isotope ratio of interest, $^{*}R_o$ is the initial isotope ratio, f is the fraction remaining, and $^{*}\alpha_{evap}$ is the fractionation factor. When all the moisture in the vapor is derived from the evaporating water body, $^{*}\alpha_{evap}$ can be calculated using[3]:

$$ {}^{*}\alpha_{evap} = {}^{*}\alpha_{eq}\left({}^{*}\alpha_{diff}(1-RH)+RH\right) \quad (8) $$

where $^{*}\alpha_{eq}$ is the temperature-dependent kinetic fractionation factor[2] and $^{*}\alpha_{diff}$ is the diffusional fractionation factor, which is dependent on the turbulence immediately above the surface of the evaporating pan[3]:

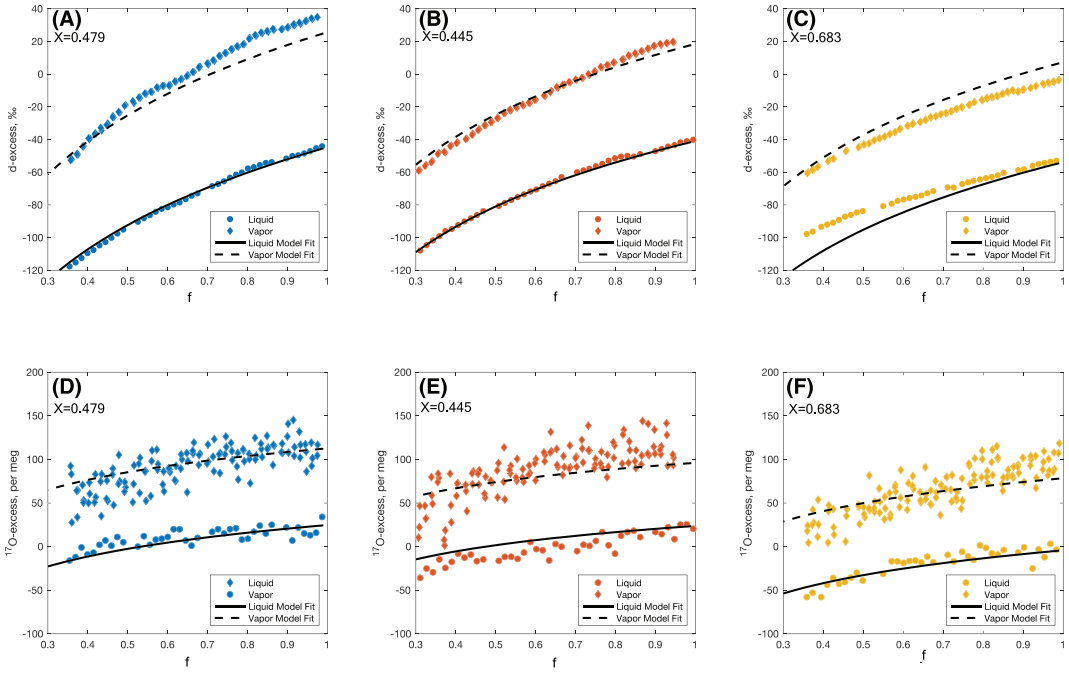

FIGURE 7 Liquid and vapor evolution for the derived parameters d-excess (A–C) and ^{17}O-excess (D–F) for each experiment, with the turbulence parameter, X, as calculated by Equation 9. Experiments conducted at A, D, 26.6% and B, E, 34.2% RH show very close agreement between experimental data and model predictions. The 55.5% RH experiment (C, F) shows a slight deviation between predicted values of the d-excess in both the liquid and the vapor and the experimental data, and this is discussed in the main text

$$^{18}\alpha_{diff} = 1.0283^{X} \quad (9)$$

The turbulence parameter, X, varies from 1 in purely diffusional regimes to 0 when the flow is entirely turbulent.[9] In the chamber experiments described above, the RH is controlled by varying the speed at which the dry gas can flow through the chamber, resulting in a different turbulence parameter, X, for each experiment. Using the results from Equation 6 and Equations 8 and 9, a value for X is produced for each experiment. The values of X are 0.497, 0.445, and 0.705 for the 26.6%, 34.2%, and 55.5% RH experiments, respectively.

To calculate model trends for the derived parameters, the values of $^{17}\alpha_{diff}$ and $^{2}\alpha_{diff}$ must be known. The value of $^{17}\alpha_{diff}$ is directly related to the result of Equation 9[3]:

$$^{17}\alpha_{diff} = {}^{18}\alpha_{diff}{}^{\theta_{diff}} \quad (10)$$

where $\theta_{diff} = 0.5185$. $^{2}\alpha_{diff}$ is calculated using[5]:

$$^{2}\alpha_{diff} = (1.25 - 0.02\,T)\left({}^{18}\alpha_{diff} - 1\right) + 1 \quad (11)$$

where T is the temperature in °C. Using Equations 10 and 11, model evaporative trends for each isotope species and the derived parameters, d-excess and ^{17}O-excess, are calculated for each experiment. Figure 7 highlights the general agreement between model trends for the d-excess and ^{17}O-excess, and the liquid and vapor experimental data.

At higher RH, the agreement between the model prediction for d-excess in the liquid and the vapor phases and the experimental data is poorer than that of the two lower RH experiments. Whilst initially in good agreement, the liquid phase evolves to be ~15‰ greater than the model-predicted equivalent and the vapor phase. In addition, the initial value for the d-excess of the vapor is lower than the predicted values by ~10‰ and evolves parallel to the liquid data. This offset is probably because vapor measurements are more significantly affected by the longer residence time of the carrier gas in the chamber at higher RH.

4 | FUTURE WORK

Understanding the isotopic evolution of water as it undergoes evaporation is fundamental for interpretation of modern and paleohydrologic data.[29,30] For example, the isotope mass balance is often used to estimate the relative inputs and losses of water in modern lakes, and is one of the few methods available for constraining evaporation. Stable isotopes of minerals formed in lakes are often used to reconstruct past changes in hydrology and climate. Evaporation experiments are a basic but useful tool to understand how the isotopic composition of water evolves as it undergoes evaporation. Previous work has been successful at revealing fundamental isotopic relationships, but experimental designs have not always been ideal for monitoring more complex evaporative trends.[2–9] Our study outlines a sampling and measuring strategy for evaporation experiments that provides highly precise results at a sampling rate that allows for the determination of isotopic trends with very narrow confidence limits about the slopes of these trends.

Although we have demonstrated the method with a very simple design where a pan of water of fixed dimensions undergoes evaporation and sets the RH in the chamber, more complicated evaporation experiments can be conducted with intricate designs of the evaporation pan and introducing an additional source of water vapor to the chamber of known isotopic composition. For example, we plan to conduct future experiments using 3D-printed models of lake basins to explore the response of the isotopic composition of the evaporating water as the surface-area-to-volume changes. In the experiments highlighted above, a crude method for controlling the RH between experiments was used for simplicity of experimental design. However, controlling for this parameter between experiments is of significant importance especially when attempting to model real-world systems (where X can be estimated from existing datasets). Transient experiments can also be conducted to simulate changes in the hydrologic balance of lake basins or sensitivity to changes in the conditions of evaporation: temperature, relative humidity, or wind regimes. Most natural systems do not undergo evaporation into a perfectly dry atmosphere and thus introducing water vapor of known isotope composition into the evaporation chamber can more realistically simulate the conditions of evaporation.

We emphasize the importance of evaporation chamber design to address the question of interest. Our large-volume chamber was designed for large-scale evaporation experiments using lake basin models but is not ideal for other applications. Carefully controlling and monitoring the conditions of the evaporation experiment (temperature, humidity, turbulence) are necessary to test numerical models of the system. The experimental design must consider the volume of the evaporation chamber, flow rate and replacement time of vapor in the chamber, turbulence above the evaporating fluid, mixing (homogeneity) of vapor in the chamber, and prevention of condensation. Once carefully accounted for, the sampling and measuring methodology outlined here offers a powerful tool for testing theoretical models of evaporation and conducting experiments to simulate natural hydrological systems.

ACKNOWLEDGMENTS

The authors thank Robert Mulvaney of the British Antarctic Survey for discussions about continuous flow analysis and loaning them the equipment to get started. They are also grateful to Fernando Gázquez who carefully read the manuscript and suggested improvements. They also thank two anonymous reviewers for their comments which greatly improved the paper. The work was supported by the ERC WHIM project (#339694) to DAH and the NERC DTP studentship (NE/L002507/1) awarded to MPB.

PEER REVIEW

The peer review history for this article is available at https://publons.com/publon/10.1002/rcm.9078.

ORCID

Matthew P. Brady https://orcid.org/0000-0003-2674-6946

David A. Hodell https://orcid.org/0000-0001-8537-1588

REFERENCES

1. Craig H, Gordon LI. Deuterium and oxygen 18 variations in the ocean and marine atmosphere. In: Tongiorgi E, ed. *Stable Isotopes in Oceanographic Studies and Paleotemperatures*. Pisa: Laboratorio di Geologia Nucleare; 1965.
2. Merlivat L. Molecular diffusivities of $H_2{}^{16}O$, HD ^{16}O, and $H_2{}^{16}O$ in gases. *J Chem Phys*. 1978;69(6):2864. https://doi.org/10.1063/1.436884
3. Barkan E, Luz B. Diffusivity fractionations of $H_2{}^{16}O/H_2{}^{17}O$ and $H_2{}^{16}O/H_2{}^{18}O$ in air and their implications for isotope hydrology. *Rapid Commun Mass Spectrom*. 2007;21(18):2999-3005. https://doi.org/10.1002/rcm.3180
4. Hu H, Bao W, Wang T, Qu S. Experimental study on stable isotopic fractionation of evaporating water under varying temperature. *Water Sci Eng*. 2009;2(2):11-18. https://doi.org/10.3882/j.issn.1674-2370.2009.02.002
5. Luz B, Barkan E, Yam R, Shemesh A. Fractionation of oxygen and hydrogen isotopes in evaporating water. *Geochim Cosmochim Acta*. 2009;73(22):6697-6703. https://doi.org/10.1016/j.gca.2009.08.008
6. Surma J, Assonov S, Herwartz D, Voigt C, Staubwasser M. The evolution of ^{17}O-excess in surface water of the arid environment during recharge and evaporation. *Sci Rep*. 2018;8(1):4972. https://doi.org/10.1038/s41598-018-23151-6
7. Surma J, Assonov S, Bolourchi M, Staubwasser M. Triple oxygen isotope signatures in evaporated water bodies from the Sistan Oasis, Iran. *Geophys Res Lett*. 2015;42(20):8456-8462. https://doi.org/10.1002/2015GL066475
8. Skrzypek G, Mydłowski A, Dogramaci S, Hedley P, Gibson JJ, Grierson PF. Estimation of evaporative loss based on the stable isotope composition of water using Hydrocalculator. *J Hydrol*. 2015;523:781-789. https://doi.org/10.1016/j.jhydrol.2015.02.010
9. Gonfiantini R, Wassenaar LI, Araguas-Araguas L, Aggarwal PK. A unified Craig-Gordon isotope model of stable hydrogen and oxygen isotope fractionation during fresh or saltwater evaporation. *Geochim Cosmochim Acta*. 2018;235:224-236. https://doi.org/10.1016/j.gca.2018.05.020
10. Cappa CD, Hendricks MB, DePaolo DJ, Cohen RC. Isotopic fractionation of water during evaporation. *J Geophys Res: Atmospheres*. 2003;108(D16). https://doi.org/10.1029/2003JD003597
11. Epstein S, Mayeda T. Variation of O^{18} content of waters from natural sources. *Geochim Cosmochim Acta*. 1953;4(5):213-224. https://doi.org/10.1016/0016-7037(53)90051-9
12. Gehre M, Hoefling R, Kowski P, Strauch G. Sample preparation device for quantitative hydrogen isotope analysis using chromium metal. *Anal Chem*. 1996;68(24):4414-4417. https://doi.org/10.1021/ac9606766
13. Vaughn BH, White JWC, Delmotte M, Trolier M, Cattani O, Stievenard M. An automated system for hydrogen isotope analysis of water. *Chem Geol*. 1998;152(3–4):309-319. https://doi.org/10.1016/s0009-2541(98)00117-x
14. Barkan E, Luz B. High precision measurements of $^{17}O/^{16}O$ and $^{18}O/^{16}O$ ratios in H_2O. *Rapid Commun Mass Spectrom*. 2005;19(24):3737-3742. https://doi.org/10.1002/rcm.2250
15. Steig E, Gkinis V, Schauer A, et al. Calibrated high-precision ^{17}O-excess measurements using cavity ring-down spectroscopy with laser-current-tuned cavity resonance. *Atmos Meas Tech*. 2014;7(8):2421-2435. https://doi.org/10.5194/amt-7-2421-2014
16. Luz B, Barkan E. Variations of 17O/16O and $^{18}O/^{16}O$ in meteoric waters. *Geochim Cosmochim Acta*. 2010;74(22):6276-6286. https://doi.org/10.1016/j.gca.2010.08.016
17. Schoenemann SW, Schauer AJ, Steig EJ. Measurement of SLAP2 and GISP $\delta^{17}O$ and proposed VSMOW-SLAP normalization for $\delta^{17}O$ and $^{17}O_{excess}$. *Rapid Commun Mass Spectrom*. 2013;27(5):582-590. https://doi.org/10.1002/rcm.6486
18. Allan DW. Statistics of atomic frequency standards. *Proc IEEE*. 1966;54(2):221-230. https://doi.org/10.1109/proc.1966.4634
19. Gkinis V, Popp TJ, Johnsen SJ, Blunier T. A continuous stream flash evaporator for the calibration of an IR cavity ring-down spectrometer for the isotopic analysis of water. *Isot Environ Health Stud*. 2010;46(4):463-475. https://doi.org/10.1080/10256016.2010.538052
20. Schauer AJ, Schoenemann SW, Steig EJ. Routine high-precision analysis of triple water-isotope ratios using cavity ring-down spectroscopy. *Rapid Commun Mass Spectrom*. 2016;30(18):2059-2069. https://doi.org/10.1002/rcm.7682
21. Jones TR, White JWC, Steig EJ, et al. Improved methodologies for continuous-flow analysis of stable water isotopes in ice cores. *Atmos Meas Tech*. 2017;10(2):617-632. https://doi.org/10.5194/amt-10-617-2017
22. Criss RE. *The Principles of Stable Isotope Distribution*. Oxford: Oxford University Press; 1999.
23. Evans NP, Bauska TK, Gázquez-Sánchez F, Brenner M, Curtis JH, Hodell DA. Quantification of drought during the collapse of the classic Maya civilization. *Science*. 2018;361(6401):498-501. https://doi.org/10.1126/science.aas9871
24. Gázquez F, Morellón M, Bauska T, et al. Triple oxygen and hydrogen isotopes of gypsum hydration water for quantitative paleo-humidity reconstruction. *Earth Planet Sci Lett*. 2018;481:177-188. https://doi.org/10.1016/j.epsl.2017.10.020
25. Gonfiantini R, Wassenaar LI, Araguas-Araguas L. Stable isotope fractionations in the evaporation of water: The wind effect. *Hydrol Process*. 2020;34(16):3596-3607. https://doi.org/10.1002/hyp.13804
26. Bao H, Cao X, Hayles JA. Triple oxygen isotopes: Fundamental relationships and applications. *Annu Rev Earth Planet Sci*. 2016;44(1):463-492. https://doi.org/10.1146/annurev-earth-060115-012340
27. Gázquez F, Calaforra J, Evans NP, Hodell DA. Using stable isotopes ($\delta^{17}O$, $\delta^{18}O$ and δD) of gypsum hydration water to ascertain the role of water condensation in the formation of subaerial gypsum speleothems. *Chem Geol*. 2017;452:34-46. https://doi.org/10.1016/j.chemgeo.2017.01.021
28. Uemura R, Barkan E, Abe O, Luz B. Triple isotope composition of oxygen in atmospheric water vapor. *GeophysRes Lett*. 2010;47(4):L04402. https://doi.org/10.1029/2009GL041960
29. Surma J, Assonov S, Staubwasser M. Triple oxygen isotope systematics in the hydrological cycle. *Rev Mineral Geochem*. 2021;86:401-428.
30. Aron PG, Levin NE, Beverly EJ, et al. Triple oxygen isotopes in the water cycle. *Chem Geol*. 2020:120026. https://doi.org/10.1016/j.chemgeo.2020.120026

SUPPORTING INFORMATION

Additional supporting information may be found online in the Supporting Information section at the end of this article.

How to cite this article: Brady MP, Hodell DA. Continuous and simultaneous measurement of triple-oxygen and hydrogen isotopes of liquid and vapor during evaporation experiments. *Rapid Commun Mass Spectrom*. 2021;35:e9078. https://doi.org/10.1002/rcm.9078